Fast-sampling fast-ion D-alpha measurement using multi-anode photomultiplier tube in large helical device

メタデータ	言語: English 出版者: AIP Publishing 公開日: 2023-10-12 キーワード (Ja): キーワード (En): 作成者: KAWACHI, Yuichi, OGAWA, Kunihiro, OSAKABE, Masaki, KAWAMOTO, Yasuko, ISOBE, Mitsutaka, IDA, Katsumi メールアドレス: 所属:
URL	http://hdl.handle.net/10655/0002000080

This work is licensed under a Creative Commons Attribution 4.0 International License.

A fast sampling fast ion D-alpha measurement using a multi-anode photomultiplier tube on the large helical device.

Y. Kawachi,[1] K. Ogawa,[2,3] M. Osakabe,[2,3] Y. Kawamoto,[2,3] M. Isobe,[2,3] and K. Ida[2,3]
[1)]*Department of Electronics, Kyoto Institute of Technology, Matsugasaki, Sakyo Ward, Kyoto 606-8585, Japan*
[2)]*National Institute for Fusion Science, National Institutes of Natural Sciences, Toki, Gifu 509-5292, Japan*
[3)]*The Graduate University for Advanced Studies, SOKENDAI, Toki, Japan*

(*Electronic mail: kawachi@kit.ac.jp)

(Dated: 28 April 2023)

A fast sampling fast ion D-alpha (F-FIDA) measurement has been developed on the large helical device (LHD) in order to investigate fast ions dynamics associated with helically trapped fast ions driven MHD bursts. The F-FIDA consists of a multi-anode photomultiplier tube (PMT) and achieves sampling rate of 10 kHz. During the deuterium experiment campaign in 2022, the F-FIDA measured the spectrum of perpendicular fast ions using perpendicular lines of sight. We compared the F-FIDA with conventional FIDA using EMCCD and confirmed that the time-averaged images were generally consistent between the F-FIDA and the conventional FIDA. The statistical properties of the temporal evolution associated with MHD bursts were analyzed using conditional sampling technique. The results showed that the PMT signal varied differently in different spatial and wavelength channels. Although the signal-to-noise ratio is poor and there is room for improvement, it could provide useful information for studies on the phase-space dynamics of fast ions.

I. INTRODUCTION

Understanding how fast ions behave in phase space (i.e. a space consisting of velocity space and position space) is an important issue for realization of efficient fusion burning plasma. To measure the behavior of fast ions in phase space, fast ion D-alpha (FIDA) measurements have been developed in various devices[1–7]. FIDA is a kind of charge exchange recombination spectroscopy utilizing Doppler shifted Balmer-alpha light of deuterium (also can be utilizing hydrogen[8]) to estimate energy distribution of fast ions[9]. Various FIDA measurements have been developed for different purposes, such as imaging FIDA[10] and tomographic FIDA[11].

So far, the study of fast ions has been used for time-averaged or slow phenomena, but we are now encountering a phase for understanding faster phenomena related to collisionless wave particle interactions, such as energetic particle driven geodesic acoustic mode[12] and fish-bone instability[13], to investigate the alpha particle channeling for self-ignition. For examples of recent progress of the fast ion measurements, a time resolved neutral particle analyzer revealed the slowing down process related to toroidal Alfén eigen mode[14]. Lately, helically trapped fast ions induced tongue deformation[15–18] and subsequent MHD bursts have been studied in the larger helical device (LHD)[19,20]. The transport of fast ions associated with the MHD burst was found by multi-code line-integrated neutron measurements[21,22], which is also a time resolved fast particle diagnostic. The phase-space dynamics of bulk ions has also been firstly observed by fast charge exchange spectroscopy[18]. To comprehensively understand the phase-space dynamics from bulk ions to fast ions during the MHD bursts, a FIDA system with high spatial, energy, and temporal resolution is required.

This paper presents a newly installed FIDA which has 100 times higher temporal resolution than a conventional FIDA system,in the LHD. The new FIDA system utilizes a multi-anode PMT aiming to improve temporal resolution at the expense of spatial and wavelength resolutions, hereinafter referred to fast sampling FIDA (F-FIDA). Section II describes the F-FIDA system and the comparison with the conventional FIDA. Section III shows experimental conditions with appearance of helically trapped fast ions induced MHD bursts and initial results of the F-FIDA in the experimental condition. Finally, we summarize the F-FIDA and the observation results in Section IV.

II. F-FIDA MEASUREMENT SYSTEM

Figure 1 (a) shows a simplified schematic views of F-FIDA system. The LHD has three of tangential, and two of perpendicular neutral beam (NB) injection. In this study, we utilized perpendicular NB injection NB #4, as a fast ion source well the active neutral particles source for the F-FIDA measurement. NB #4 is modulated to measure background of the FIDA spectrum, To observe perpendicular fast ions, we used perpendicular lines of sight reflected by a pair of upper and lower curved mirrors[8,23,24]. The reflected light is collected to optical fibers, and transmitted to a spectrometer system (BUNKOKEIKI, FLP-200_VPH), as shown in Figure 1(b). The center wavelength is set to 651.3 nm. The 30% of spectral light transmitted through beam splitter to a electron multiplying charged-coupled device (EMCCD) (iXon 897, ANDOR), which was used for conventional FIDA images. The typical exposure time of the measurement is 7 ms and the sampling rate was set to 100 Hz. The number of pixels is set to 32 pixels in height and 512 pixels in width.

The 70% of spectral light image is redirected by a beam splitter, and magnified by a lens by a factor of two. Then, it is detected as current signal by a 8×8t channel multi-anode photomultiplier tube (H7546A-20) biased by high voltage module (RPH-034, HAYASHIREPIC). The detected current sig-

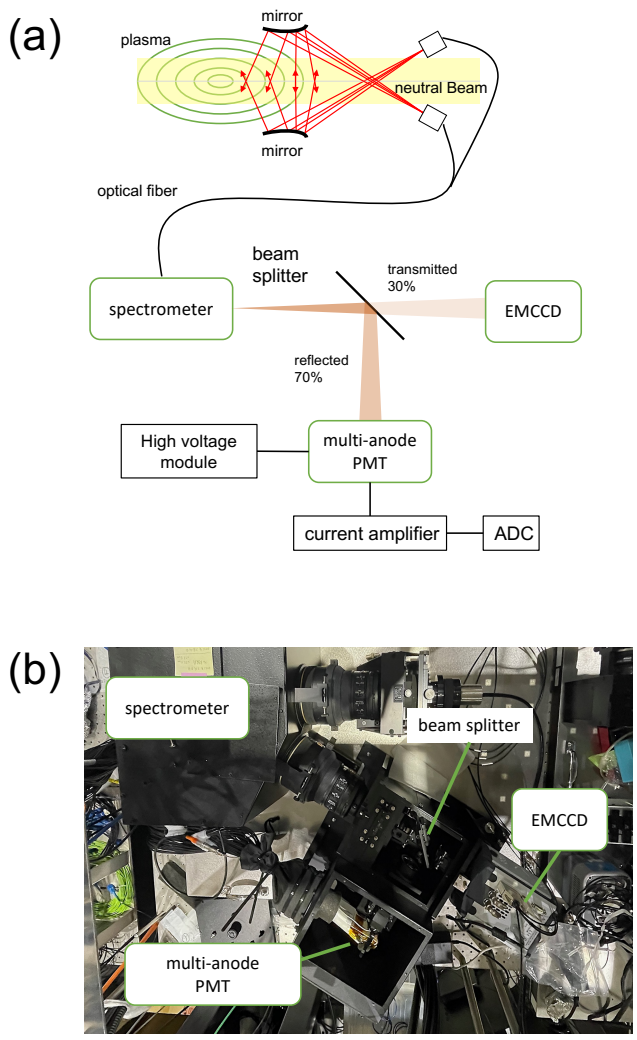

FIG. 1. (a) Simplified schematic views of the F-FIDA measurement. (b) A photograph of an optical system of the F-FIDA

nal is amplified and converted to voltage signal by a current amplifier unit (C7319, Hamamatsu Photonics). The 32 channels of current amplifiers was prepared in this experimental campaign. The bandwidth of the current amplifier is set to 200 kHz and the gain is set to 10^6 for channels that detect cold D-alpha components and 10^7 for all others. To reduce noise, digital decimating is performed at a sampling rate of 10 kHz. We note that since the size of one channel of the multi-anode PMT element is larger than that of the EMCCD pixels (even though the image is enlarged by a factor of two), the light integrated over 64 channels in the horizontal direction and 4 channels in the vertical direction is detected by each PMT element.

The typical time averaged conventional FIDA spectral images in the experiment for the shot #183661 are shown in Figures 2 (a)-(c). The 32 pixels in height and the 512 pixels in width of EMCCD correspond to measurement points of major radius (R = 3.817-4.8172 m, that is $r_{\rm eff}/a_{99}$ = 0.19-1.1) and λ = 646.92-655.66 nm of wavelength of the spectrum. Here, $r_{\rm eff}$ is the effective minor radius of the plasma and the a_{99} is the minor radius where 99% of kinetic energy is confined. We note that spatial resolution is inhomogeneous at each radial position because the line of sight cross many flux surfaces[24]. The charge exchange driven perpendicular fast hydrogen H-alpha spectra is simulated in Ref.[8]. Based on this, the energy dependence of the perpendicular fast D-alpha spectra is roughly estimated, such as $\lambda \sim 651$ nm for 80 keV and $\lambda \sim 653$ nm for 40 keV. In this experiment, the NBs #4 and #5 produce about 65 keV and 80 keV beam ions, respectively and the beam ions are considered to be helically trapped. Multiple peaks at $R \approx 4.6-4.7$ m ($r_{\rm eff}/a_{99} \approx 1.01-1.07$) where is near X-point and almost outsides of the last closed flux surface), indicate prompt loss fast ions for three energy components of $E_{\rm NB\#4}$, $E_{\rm NB\#4}/2$, $E_{\rm NB\#4}/3$. Here, $E_{\rm NB\#4}$ is fast ions energy produced by NB#4. The spectrum around $\lambda \sim$ 650.34-653.76 nm has the information for fast ions while around $\lambda \sim 655$ nm) indicates cold D-alpha components. A sharp peak only observed at around $\lambda = 650$ nm in background (Fig. 2 (a)) indicates impurity oxygen ion line ($O^{5+}, \lambda = 650.024$ nm). For more information of the interpretation of perpendicular FIDA spectrum in LHD, see Ref.[8].

Figures 2 (d)-(f) show the typical time averaged spectral images obtained by F-FIDA. Each dashed squares indicates multi-anode PMT channels. Here, the 32 channels of F-FIDA chosen as five or six of wavenumber channels and six of positional channels. Compared to the conventional FIDA image, we can see that the F-FIDA image is generally similar, especially in the channels showing cold ions (i.e. such as ch 5 and ch 10) and prompt loss of fast ions (i.e. such as ch 22-24). We note that a previous attempt of F-FIDA using PMT was made at NSTX[2] and DIII-D[25], which appears to be similar to this study. The previous studies used band-passed signal in wavenumber domain to improve time resolution. While the F-FIDA measurement is partially integrated in position and wavenumber pixels. Therefore, the F-FIDA has advantage of wavenumber resolution.

III. EXPERIMENTAL RESULTS

The F-FIDA measurements applied to high ion temperature discharges during the 23rd LHD experimental campaign. In the discharges, low density deuterium plasma is sustained by fueling by deuterium NBs#1-3 in the discharge with wall conditioning by ion cyclotron heating, and heated by the perpendicular deuterium NBs#4-5. The typical time evolution for the shot #183661 is shown in Figures 3. It is considered that, the pressure gradient of helically trapped fast ions drives the localized deformation (referred to Tongue deformation), then the rotating MHD burst with tearing parity and the RF intensity bursts are appeared[16], as shown in Figures 3 (b) and (d). The phase space dynamics of the bulk ions were observed as deviation of Maxwell distribution due to the Landau damping[18]. On the other hands, the phase space dynamics of fast ions could be related the RF bursts. Indeed, neutron emission rate, which is related to fusion reaction between fast ions and thermal balk ions, changes corresponding to the bursts.

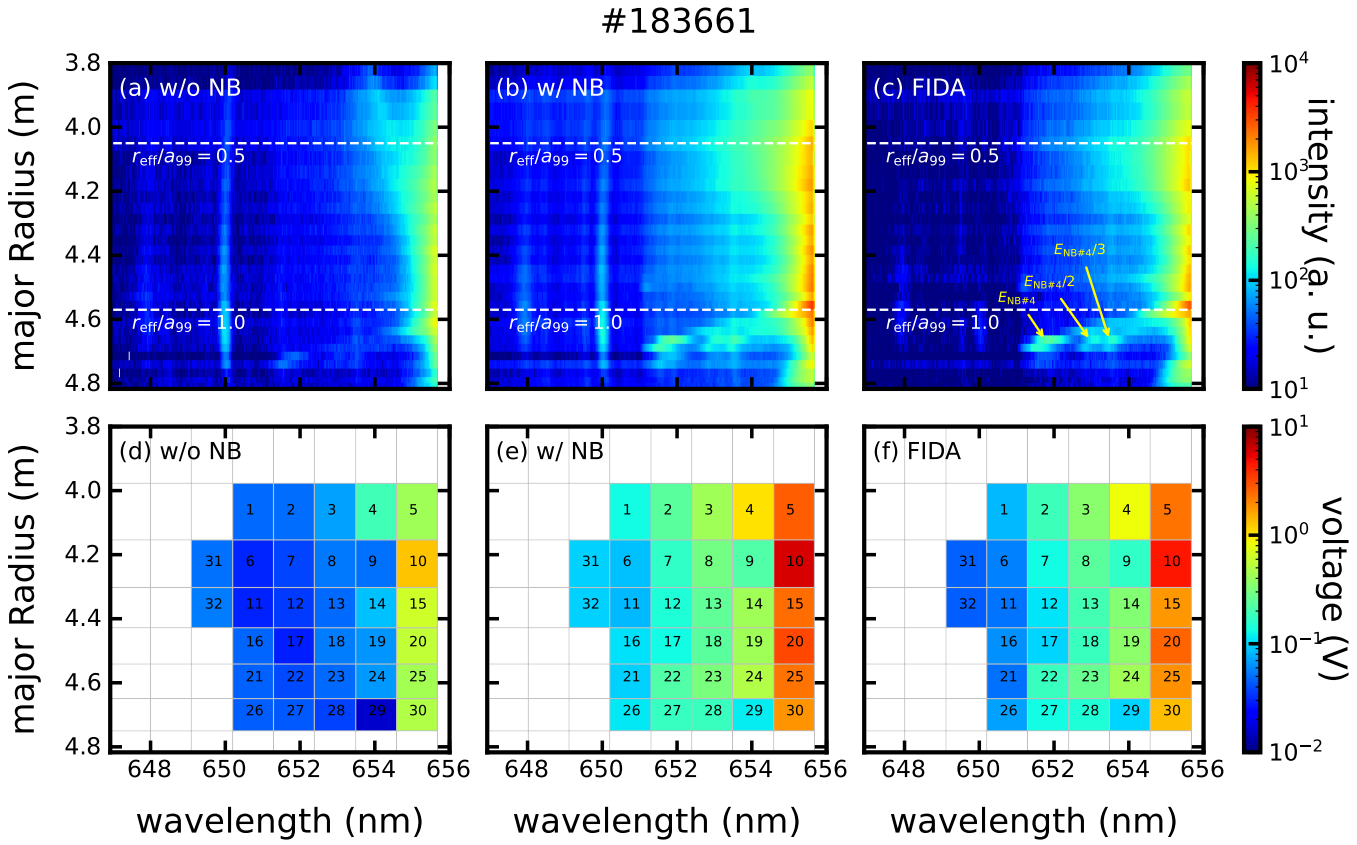

FIG. 2. Comparison of time averaged spectral images of the conventional FIDA (a)-(c) and the F-FIDA (d)-(f) for the shot #183661. The left column shows the background spectrum, the middle column shows the spectrum when NB #4 is injected. The right column shows the FIDA spectrum obtained by subtracting the background spectrum from the spectrum with NB#4 .

The F-FIDA have potential to investigate more detailed phase space dynamics because of wavelength- and space-resolved local measurement. Multi-anode PMT signals of F-FIDA at R = 3.88 m are shown in Figure 3 (e). It can be seen that the PMT signals immediately decrease as NB #4 is turned off. Unfortunately, it is difficult to see the changes corresponding to the bursts from the raw PMT signal.

In order to increase the signal-to-noise ratio of the F-FIDA measurement, conditional sampling technique are applied. Conditional sampling is a great tool for improve signal to noise ratio to analyze bursty quasi-periodic phenomena. This analysis uses the RF intensity signal as the reference signal. When the RF signal exceeds a threshold value, it is detected as the time when the burst is excited. Then, many ensembles of time series are re-sampled from original time series at each time lag from the burst exited timing, and averaged (or other statistical processing), represented as $\langle x \rangle(\tau) = \frac{1}{N}\sum_i x(t_i + \tau)$. Here $x(t)$ is the original time series signal, N is number of ensembles of the bursts, t_i is i-th burst excited timing, and τ is time delay from the burst excited timing. Finally, we obtain the statistical time evolution corresponding to the burst. An ensemble of 736 bursts from 13 discharges was used to calculate the conditional mean in this study.

The conditional averaged results are shown in Figures 4. Concerning the time evolution of the magnetic fluctuation (Fig. 4 (b)), single pulse like waveforms is seen, which indicates the localized tongue deformation. While the MHD burst signal after the tongue deformation is suppressed by the conditional averaging, because the burst signals are sinusoidal-like waveform and have different phases for each ensemble.

Figures 4 (c)-(h) show the conditional averaged PMT signal of the F-FIDA at $R = 4.24$ m. It can be seen that all channels of the PMT signal statistically changes with the RF burst, although signal to noise ratio is still large after conditional averaging. For clarity, the low-pass filtered signal (< 5 kHz) is also plotted together in Figures 4 (c)-(h). The PMT signal of high energy side, corresponding to the fast D-alpha energy of 40-80 keV, shows a about 10-15% decreases after the burst onset, as shown in Figures 4 (d)-(f). In other words, the fast ion beam component at the core plasma was reduced with the burst. The decreases of the lowest energy one of three PMT signal (represented in Figure 4 (f)) is lagged by 2 ms compared with others. After the burst ends, the PMT signal on the high-energy side begins to recover. The PMT signal on the low energy side, estimated to be below 20 keV, increases at about 15% after the burst onset, represented in Figure 4 (g). In addition, the increase seems to have two phase of rapid and gradual phases. Then, the PMT signal on the low energy side decreases after the bursts.

Here, we discuss other signals than fast D-alpha. Fig-

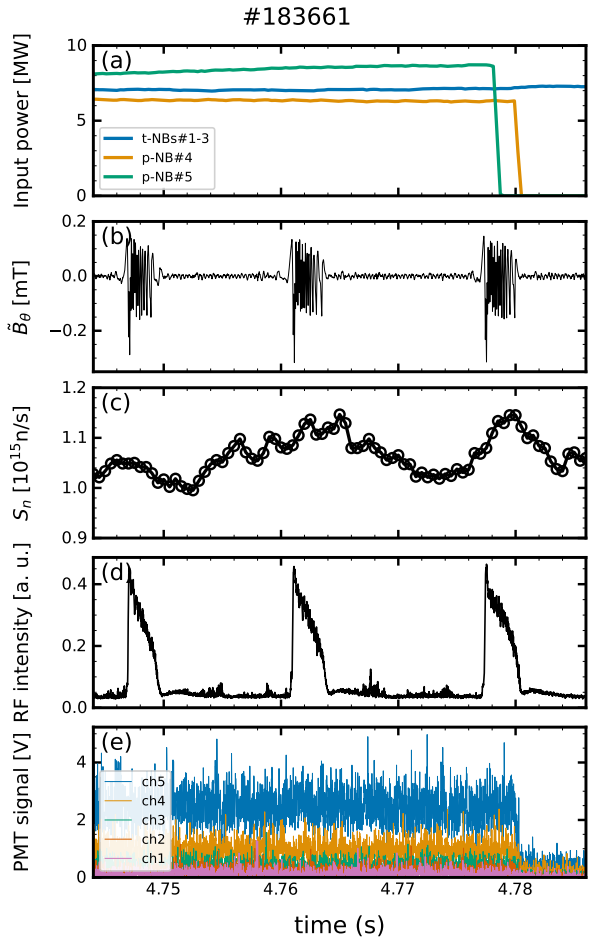

FIG. 3. Time evolution for the shot #183661 of (a) neutral beam injection power, (b) magnetic field fluctuation, (c) neutron neutron emission rate, (d) RF intensity, and (e) multi-anode PMT signal in a discharge with the MHD burst. Dashed vertical line in each figure indicates the bursts reference timing

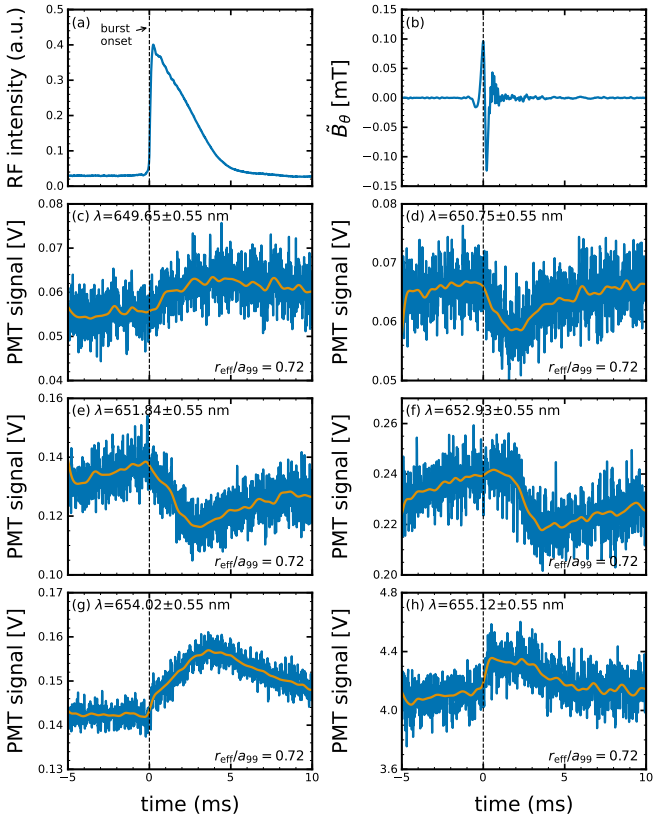

FIG. 4. Conditional averaged waveforms of (a) RF intensity, (b) magnetic fluctuation, and (c)-(h) PMT signals of F-FIDA at around $R = 4.24$ m ($r_{\rm eff}/a_{99} = 0.72$) where fast ions are helically trapped. The λ in (c)-(h) denotes the wavelength at which each PMT channel is measured.

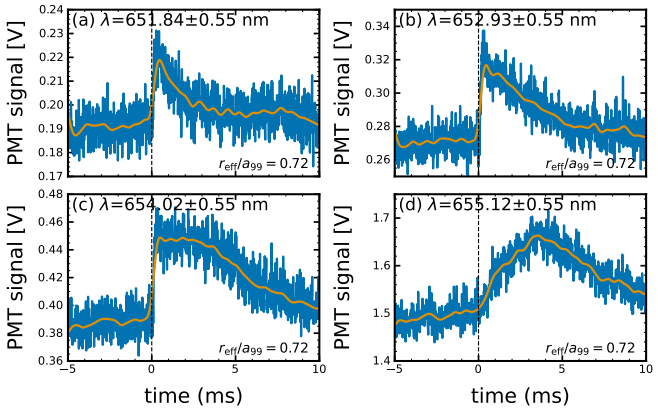

FIG. 5. Conditional averaged waveforms of PMT signals of F-FIDA at around $R = 4.60$ m ($r_{\rm eff}/a_{99} = 1.02$). The λ in (a)-(d) denotes the wavelength at which each PMT channel is measured.

ure 4 (c) represent the PMT signal of the impurity oxygen line O^{5+}. It seems to increases gradually at, which is different from the behavior of other PMT signals on the high energy side. Concerning with the cold D-alpha component shown in Figure 4 (h), the signal was observed to increase slightly and quickly by about 5%. This behavior does not resemble the behavior on the low energy side, which suggests that it is not a fast ion but rather the bulk cold D-alpha behavior.

Figures 5 (a)-(d) show the conditional averaged PMT signal of the F-FIDA at $R = 4.60$ m where is near the last closed flux surface and X-point ($r_{\rm eff}/a_{99} = 1.02$). Faster increases of the PMT signals are observed than that at $R = 4.24$ m (Figs. 4(e)-(h)). This indicates that the prompt loss ions rapidly increases, because he peaks of prompt loss signal should be detected at $\lambda = 651.84$-654.02 nm, as shown in Figures 2. These results suggest that the RF bursts associated with this phenomenon are due to prompt loss ions. The PMT signal at wavelengths where there would be no prompt loss certainly behaves differently from other signals, and is assumed to be the signal change related to cold D-alpha. Another interesting result is that the decay time after the increase varies with wavelength for prompt loss.

IV. SUMMARY

We have developed a fast sampling fast ion D-alpha measurement on the LHD. The F-FIDA consists of a multi-anode PMT and has 8×8 wavelength and spatial channels and the 200 kHz of bandwidth. Comparison of time-averaged spectrum confirms that the F-FIDA obtained a signal that is generally agree with a conventional FIDA. Initial results associated with the MHD bursts induced by helically trapped fast deuterium were obtained in the LHD deuterium experiment campaign in 2022. We observed the behavior of the PMT signal at different wavelengths would be indicating for impurity ions, cold ions, and fast ions. Our results suggests that: the fast ion beam at the core was decreased while the prompt loss fast of ions was increased ,with the burst. Signal to noise ratio is reduced by using the conditional sampling but it found that the signal to noise ratio still large. Further improvement of the signal-to-noise ratio, for example, by bundling the fiber to collect more light, remains a future work. In order to interpret the changes of the F-FIDA signal, comparison and validation studies with simulations will be conducted.

V. ACKNOWLEDGEMENT

We would like to thank the LHD experiment group for their cooperation in the LHD operations and experiments. This work was supported by JSPS KAKENHI Grant Numbers JP21H04973. The datasets of for the current study are available to the public in the LHD data repository server of the National Institute for Fusion Science (NIFS) via `https://doi.org/10.57451/lhd.analyzed-data`.

[1] W. W. Heidbrink, Review of Scientific Instruments **81**, 10D727 (2010).
[2] M. Podestà, W. W. Heidbrink, R. E. Bell, and R. Feder, Review of Scientific Instruments **79**, 10E521 (2008), publisher: American Institute of Physics.
[3] E. Delabie, R. J. E. Jaspers, M. G. von Hellermann, S. K. Nielsen, and O. Marchuk, Review of Scientific Instruments **79**, 10E522 (2008), publisher: American Institute of Physics.
[4] B. Geiger, M. Garcia-Munoz, W. W. Heidbrink, R. M. McDermott, G. Tardini, R. Dux, R. Fischer, V. Igochine, and t. A. U. Team, Plasma Physics and Controlled Fusion **53**, 065010 (2011).
[5] C. A. Michael, N. Conway, B. Crowley, O. Jones, W. W. Heidbrink, S. Pinches, E. Braeken, R. Akers, C. Challis, M. Turnyanskiy, A. Patel, D. Muir, R. Gaffka, and S. Bailey, Plasma Physics and Controlled Fusion **55**, 095007 (2013), publisher: IOP Publishing.
[6] Y. M. Hou, C. R. Wu, J. Huang, W. W. Heidbrink, M. G. von Hellermann, Z. Xu, Z. Jin, J. F. Chang, Y. B. Zhu, W. Gao, Y. J. Chen, B. Lyu, R. J. Hu, P. F. Zhang, L. Zhang, W. Gao, Z. W. Wu, Y. Yu, M. Y. Ye, and EAST Team, Review of Scientific Instruments **87**, 11E552 (2016).
[7] Y. Fujiwara, S. Kamio, H. Yamaguchi, A. V. Garcia, L. Stagner, H. Nuga, R. Seki, K. Ogawa, M. Isobe, M. Yokoyama, W. W. Heidbrink, M. Osakabe, and L. E. Group, Nuclear Fusion **60**, 112014 (2020), publisher: IOP Publishing.
[8] M. Osakabe, S. Murakami, M. Yoshinuma, K. Ida, A. Whiteford, M. Goto, D. Kato, T. Kato, K. Nagaoka, T. Tokuzawa, Y. Takeiri, and O. Kaneko, Review of Scientific Instruments **79**, 10E519 (2008).
[9] W. W. Heidbrink, K. H. Burrell, Y. Luo, N. A. Pablant, and E. Ruskov, Plasma Physics and Controlled Fusion **46**, 1855 (2004).
[10] C. Marini, C. S. Collins, M. A. Van Zeeland, K. E. Thome, W. W. Heidbrink, and D. Lin, Review of Scientific Instruments **92**, 033533 (2021).
[11] M. Weiland, B. Geiger, A. S. Jacobsen, M. Reich, M. Salewski, T. Odstrčil, and t. A. U. Team, Plasma Physics and Controlled Fusion **58**, 025012 (2016), publisher: IOP Publishing.
[12] T. Ido, K. Itoh, M. Osakabe, M. Lesur, A. Shimizu, K. Ogawa, K. Toi, M. Nishiura, S. Kato, M. Sasaki, K. Ida, S. Inagaki, S.-I. Itoh, and the LHD Experiment Group, Physical Review Letters **116**, 015002 (2016), publisher: American Physical Society.
[13] K. McGuire, R. Goldston, M. Bell, M. Bitter, K. Bol, K. Brau, D. Buchenauer, T. Crowley, S. Davis, F. Dylla, H. Eubank, H. Fishman, R. Fonck, B. Grek, R. Grimm, R. Hawryluk, H. Hsuan, R. Hulse, R. Izzo, R. Kaita, S. Kaye, H. Kugel, D. Johnson, J. Manickam, D. Manos, D. Mansfield, E. Mazzucato, R. McCann, D. McCune, D. Monticello, R. Motley, D. Mueller, K. Oasa, M. Okabayashi, K. Owens, W. Park, M. Reusch, N. Sauthoff, G. Schmidt, S. Sesnic, J. Strachan, C. Surko, R. Slusher, H. Takahashi, F. Tenney, P. Thomas, H. Towner, J. Valley, and R. White, Physical Review Letters **50**, 891 (1983), publisher: American Physical Society.
[14] S. Kamio, Y. Fujiwara, K. Nagaoka, K. Ogawa, R. Seki, H. Yamaguchi, H. Nuga, M. Isobe, M. Osakabe, C. Z. Cheng, and t. L. E. Group, Nuclear Fusion **60**, 112002 (2020), publisher: IOP Publishing.
[15] K. Ida, T. Kobayashi, K. Itoh, M. Yoshinuma, T. Tokuzawa, T. Akiyama, C. Moon, H. Tsuchiya, S. Inagaki, and S.-I. Itoh, Scientific Reports **6**, 36217 (2016), number: 1 Publisher: Nature Publishing Group.
[16] K. Ida, T. Kobayashi, M. Yoshinuma, T. Akiyama, T. Tokuzawa, H. Tsuchiya, K. Itoh, and S.-I. Itoh, Scientific Reports **8**, 2804 (2018), number: 1 Publisher: Nature Publishing Group.
[17] S. Voermans, K. Ida, T. Kobayashi, M. Yoshinuma, H. Tsuchiya, T. Akiyama, and M. Emoto, Nuclear Fusion **59**, 106041 (2019), publisher: IOP Publishing.
[18] K. Ida, T. Kobayashi, M. Yoshinuma, K. Nagaoka, K. Ogawa, T. Tokuzawa, H. Nuga, and Y. Katoh, Communications Physics **5**, 1 (2022), number: 1 Publisher: Nature Publishing Group.
[19] X. D. Du, K. Toi, S. Ohdachi, M. Osakabe, T. Ido, K. Tanaka, M. Yokoyama, M. Yoshinuma, K. Ogawa, K. Y. Watanabe, T. Akiyama, M. Isobe, K. Nagaoka, T. Ozaki, S. Sakakibara, R. Seki, A. Shimizu, Y. Suzuki, H. Tsuchiya, and t. L. E. Group, Nuclear Fusion **56**, 016002 (2015), publisher: IOP Publishing.
[20] X. Du, K. Toi, S. Ohdachi, K. Watanabe, H. Takahashi, Y. Yoshimura, M. Osakabe, R. Seki, T. Nicolas, H. Tsuchiya, K. Nagaoka, K. Ogawa, K. Tanaka, M. Isobe, M. Yokoyama, M. Yoshinuma, S. Kubo, S. Sakakibara, T. Bando, T. Ido, T. Ozaki, Y. Suzuki, Y. Takemura, and LHD Experiment Group, Physical Review Letters **118**, 125001 (2017).
[21] K. Ogawa, M. Isobe, S. Sugiyama, H. Matsuura, D. A. Spong, H. Nuga, R. Seki, S. Kamio, Y. Fujiwara, H. Yamaguchi, M. Osakabe, and L. E. group, Nuclear Fusion **60**, 112011 (2020), publisher: IOP Publishing.
[22] K. Ogawa, M. Isobe, H. Nuga, S. Kamio, Y. Fujiwara, M. I. Kobayashi, S. Sangaroon, E. Takada, R. Seki, H. Yamaguchi, S. Murakami, J. Jo, and M. Osakabe, Nuclear Fusion **61**, 096035 (2021), aDS Bibcode: 2021NucFu..61i6035O.
[23] K. Ida, S. Kado, and Y. Liang, Review of Scientific Instruments **71**, 2360 (2000).
[24] M. Yoshinuma, K. Ida, M. Yokoyama, M. Osakabe, and K. Nagaoka, Fusion Science and Technology **58**, 375 (2010).
[25] C. M. Muscatello, W. W. Heidbrink, D. Taussig, and K. H. Burrell, Review of Scientific Instruments **81**, 10D316 (2010), publisher: American Institute of Physics.